RSC Advances

PAPER

View Article Online
View Journal | View Issue

Cite this: *RSC Adv.*, 2020, **10**, 33279

Near-infrared polyfluorene encapsulated in poly(ε-caprolactone) nanoparticles with remarkable large Stokes shift†

Jaruwan Joothamongkon,[a] Udom Asawapirom,[a] Raweewan Thiramanas,[a] Kulachart Jangpatarapongsa[b] and Duangporn Polpanich*[a]

Near-infrared (NIR) fluorescent dyes have attracted increasing attention as fluorescent probes in biomedical applications due to their low biological autofluorescence as well as high tissue penetration depth. However, their being hydrophobic in nature limits their clinical use as they are prone to aggregate in the physiological environment. Herein, we have designed and synthesized a novel polymeric NIR fluorescent dye and then encapsulated it into a poly(ε-caprolactone) (**PCL**) matrix by way of an emulsion–diffusion technique. The effect of the structure of the surfactant on the nanoparticle properties is investigated. Results show that polymeric surfactant, Kolliphor® P188, allows the formation of a high fluorescence intensity of the nanoparticles with the highest level homogeneity and stability. The synthesized nanoparticles show significant advantages in terms of a remarkable large stokes shift (276 nm) in the aqueous solution and excellent biocompatibility. The fabrication process is not limited to encapsulation of polymeric fluorescent dye. The synthesized NIR polymeric nanoparticles would be potentially applicable for biomedical applications.

Received 3rd July 2020
Accepted 1st September 2020

DOI: 10.1039/d0ra05809b

rsc.li/rsc-advances

1. Introduction

Near-infrared (NIR) fluorescent dyes hold great promise as imaging and therapeutic agents in biomedical applications. Due to the high sensitivity of fluorescence and minimization of unspecific background signal, this type of fluorescent dye is becoming increasingly more employed, especially in early detection and *in vivo* monitoring of disease-related pathological changes.[1–5] In this, the excitation of dye using NIR light offers the advantages of extremely low absorption and auto-fluorescence from organic tissue in the NIR spectrum window (650–900 nm), which is favorable in terms of providing an increase in penetration depth of the excitation light.[3–6] An ideal NIR fluorophore must exhibit a large Stokes shift for minimum interference between absorption and emission spectral, high molar absorption coefficient and quantum yield for intense fluorescence and good photostability in buffers or biological conditions.[7] Chemists continue to design and synthesize a variety of novel NIR dyes, including organic fluorophores such as cyanines, rhodamine analogs, 4,4-difluoro-4-bora-3*a*,4*a*-diaza-*s*-indacene (BODIPYs), squaraines, phthalocyanines, porphyrin derivatives, conjugated polymer and inorganic dyes (quantum dots).[7–11] Although the quantum dots principally present interesting alternatives, cytotoxicity and stability concerns, as well as difficulties in the reproducibility of their preparation, need to be resolved.[2,11] Compared to inorganic dyes, organic NIR fluorophores display an improvement in photophysical properties and have availability for large-scale chemical synthesis.[7,9] However, only a few of them are readily available owing to poor water solubility, which probably brings about dye accumulation in normal organs causing systemic toxicity.

Developments of encapsulation of NIR fluorophores into polymeric liposomes or nanoparticles have been extensively studied. This can direct the protection of the dyes from degradation and improve fluorescent signal (a high quantity of dye molecules per nanoparticle), biocompatibility and especially stability in a physiological condition.[1,2,12–14] Behnke *et al.* reported that the encapsulation of hydrophobic cyanine Itrybe dye into amino-modified polystyrene (PS) nanoparticles using a one-step staining procedure yielded a bright labeling probe for *in vitro* and *in vivo* sensitive tumor detection.[2,15] The presence of an amino group on the surface of particles provides an active site for antibody functionalization to improve tumor targeting efficiency.[1,2] Moreover, polymeric nanoparticles loaded with NIR dyes and anticancer agents brought about the integration of imaging and therapeutic functions to achieve the ultimate goal of simultaneous diagnosis and treatment.[7]

[a]*National Nanotechnology Center, National Science and Technology Development Agency (NSTDA), 111 Thailand Science Park, Phahonyothin Road, Khlong Nueng, Khlong Luang, Pathum Thani 12120, Thailand. E-mail: duangporn@nanotec.or.th*

[b]*Center for Innovation Development and Technology Transfer, Faculty of Medical Technology, Mahidol University, Bangkok-Noi, Bangkok 10700, Thailand*

† Electronic supplementary information (ESI) available. See DOI: 10.1039/d0ra05809b

Polyfluorene conjugated polymer and its derivatives, has gained considerable attention due to its excellent thermal and chemical stability, high photostability, and good photoluminescence yield.[16,17] However, it displays a short-wavelength photoluminescence which is not preferable for *in vivo* biomedical applications. Various low-band gap monomer units have been incorporated into the polyfluorene backbone to increase emission wavelengths to become long-wavelengths or even to the near-infrared region.[16,18,19] Meng *et al.* prepared conjugated copolymers comprising alternating fluorene and BODIPY units in the main chain.[16] The existence of BODIPY dyes gave rise to significant red shifts in the UV-vis absorption and emission spectral maxima. Later, Piyakulawat *et al.* alternately copolymerized bis-[2,2′-(5,5′-dibromo)-thienyl]-2,6-naphthalene-1,4,5,8-tetracarboxylic diimide and fluorene monomers through Suzuki type cross-coupling reactions. This led to the formation of alternated copolymers of poly{5,5′-[bis(2,2′-thiophene)-2,6-naphthalene-1,4,5,8-tetracarboxylic-*N*,*N*′-dihexyldiimide]-*alt*-[2,7-(9,9′-dioctyl)fluorene]} (PNATF) and poly{5,5'-[bis(2,2′-thiophene)-2,6-naphthalene-1,4,5,8-tetracarboxylic-*N*,*N*′-ditolyldiimide]-*alt*-[2,7-(9,9′-dioctyl)fluorene]} (PNTTOF).[19] The extension of π-conjugation throughout the main chain allowed for the tunable emission spectral maxima of the modified copolymer to the NIR wavelength region (684–770 nm).

In this study, we intended to synthesize the NIR PNATF conjugated copolymer encapsulated in a biocompatible polymer. To enhance encapsulation efficiency in polymer material by increasing hydrophobicity of the dye, molecular structure of the NIR PNATF conjugated copolymer was modified by replacing the hexyl group of naphthalene-diimide-based monomers with the ethylhexyl group to achieve poly{[2,7-(9,9′-dioctyl)fluorene]-*alt*-[5,5′-bis(2,2′-thiophene)-2,6-naphthalene-1,4,5,8-tetracarboxylic-*N*,*N*′-diethylhexyldiimide]} (**PF8NT2/6**). After being well-characterized using NMR, the modified dye was encapsulated into a poly(ε-caprolactone) (**PCL**) matrix by way of an emulsion-diffusion technique. Influence of surfactant structure on hydrodynamic diameter, zeta potential, and fluorescent properties of the **PF8NT2/6** encapsulated **PCL** (**PCL-PF8NT2/6**) nanoparticles was systematically assessed. The adjusted amount of **PF8NT2/6** in the encapsulation process was also studied to tune encapsulation efficiency (EE). Finally, as a proof-of-concept for its potential for *in vivo* applications, the cytotoxicity of the prepared particles was tested using fibroblasts.

2. Materials and methods

2.1. Materials

Bis-[2,2′-(5,5′-dibromo)-thienyl]-2,6-naphthalene-1,4,5,8-tetracarboxylic-*N*,*N*′-di(2-ethylhexyl)imide was synthesized in close analogy to method described in the literature.[19] 9,9-Dioctylfluorene-2,7-bis(trimethylborate), 97% and tetrakis(-triphenylphosphine)palladium(0), 99% ($Pd(PPh_3)_4$) were purchased from Aldrich and Acros organics, respectively. **PCL** (molecular weight 14 000 g mol^{-1}), Kolliphor® P 188 (molecular weight 7680–9510 g mol^{-1}), Tween® 80 (molecular weight 1310 g mol^{-1}) and poly(vinyl alcohol) (PVA) (99+% hydrolyzed, molecular weight 89 000–98 000 g mol^{-1}) were purchased from Sigma-Aldrich (Analytical Grade). Organic solvent including chloroform, toluene, tetrahydrofuran (THF), *n*-butanol, methanol and acetone purchased from Carlo-Erba (Analytical Grade) was used as received. Deionized (DI) water purified by PureLab Ultra water system (ELGA, UK) was used throughout the work.

2.2. Synthesis of PF8NT2/6 NIR dye

The **PF8NT2/6** NIR dye was synthesized through a Suzuki-type coupling reaction using $Pd(PPh_3)_4$ as the catalyst (Scheme 1). Bis-[2,2′-(5,5′-dibromo)-thienyl]-2,6-naphthalene-1,4,5,8-tetra carboxylic-*N*,*N*′-di(2-ethylhexyl)imide (**1**) (503.8 mg, 0.62 mmol), 9,9-dioctylfluorene-2,7-bis(trimethylborate) (**2**) (346.2 mg, 0.62 mmol) and $Pd(PPh_3)_4$ (25.7 mg, 0.02 mmol) were dissolved in a degassed mixture of aqueous Na_2CO_3 (2.5 mL; 20% w/v), *n*-butanol (2.5 mL), toluene (20 mL) and THF (20 mL). After stirring under reflux for 3 days and cooling to room temperature, aqueous HCl (2 N, 20 mL) was poured into the mixture. Extraction with chloroform was done before allowing phase separation. The organic phase containing **PF8NT2/6** NIR dye was isolated and then washed with saturated aqueous EDTA and subsequently $NaHCO_3$ solution. It was then harvested, dried over anhydrous Na_2SO_4, and evaporated solvent off. The dye was solvated in chloroform and precipitated into a mixture of methanol/aqueous HCl (2 N) (10/1, vol%), filtered, and extracted in a Soxhlet apparatus with methanol, acetone, and hexane, respectively to remove impurities and oligomers. The obtained **PF8NT2/6** was dissolved in chloroform, concentrated and precipitated in methanol/aqueous HCl (2 N) (10/1, vol%) before drying under vacuum. Yield: 0.272 g (42%).

^{1}H NMR (500 MHz, $CDCl_3$): δ 8.85 (2H), 7.63–7.75 (6H), 7.48 (2H), 7.42 (2H), 4.12 (4H), 2.05 (4H), 1.96 (2H), 1.56 (4H), 1.29–1.41 (12H), 1.10 (24H), 0.87–0.96 (12H), 0.76–0.81 (6H) (Fig. S1†). ^{13}C NMR (500 MHz, $CDCl_3$): δ 162.7, 151.9, 148.4, 140.7, 139.7, 139.6, 136.6, 132.9, 130.2, 127.6, 125.4, 125.1, 123.5, 122.7, 120.3, 120.1, 55.4, 44.6, 40.6, 37.8, 31.8, 30.6, 30.1, 29.3, 28.6, 23.9, 23.1, 22.6, 14.1, 10.6 (Fig. S2†). M_n = 18 586. M_w = 36 358. M_w/M_n = 1.96.

2.3. Preparation and characterizations of PCL-PF8NT2/6 nanoparticles

2.3.1. Preparation of PCL-PF8NT2/6 nanoparticles. The **PCL-PF8NT2/6** nanoparticles were prepared using the emulsion–diffusion method. First, chloroform (50 mL) and DI water

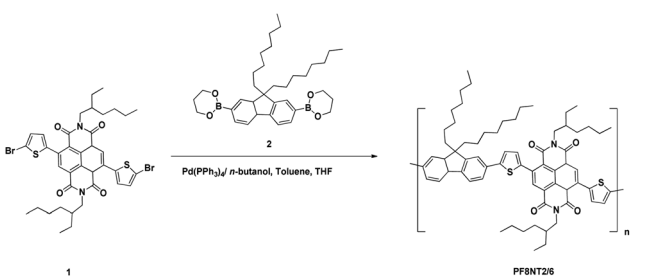

Scheme 1 Synthetic route of PF8NT2/6.

(150 mL) were mixed by mechanical stirrer for 24 hours. The mixture solvent was separated using separatory funnel to obtain the chloroform-saturated water and water-saturated chloroform which used as a continuous phase and solvent for polymer and NIR dye, respectively. Next, **PCL** (10 mg) and various amount of **PF8NT2/6** (0.00, 0.25, 0.50, 0.75, 1.00, 1.50 and 2.00 mg) were dissolved in water-saturated chloroform (3 mL). This organic phase was mixed and pre-emulsified with chloroform-saturated aqueous phase (50 mL) containing non-ionic surfactant (5.0 g), *i.e.* Kolliphor® P188, Tween® 80 or PVA, using mechanical stirrer at 500 rpm for 1 h before being emulsification with ultrasonic probe (VCX-750, SONICS, USA) at 90% amplitude for 5 minutes. DI water (200 mL) was added to the reaction while moderate stirring for 1 h at room temperature. Finally, chloroform and part of water were removed using rotary evaporator (Rotavapor R-200, Büchi, Switzerland) under reduce pressure. The obtained nanoparticles were purified by repetitive centrifugation before characterizations.

2.3.2. Characterizations. Hydrodynamic diameter, polydispersity index (PDI) and zeta potential of diluted **PCL-PF8NT2/6** nanoparticles were determined using dynamic light scattering (DLS, Zetasizer Nano Series, Malvern Instruments, UK) at 25 °C. Each sample was measured at least three times and the average values were calculated. The instrument measures the autocorrelation function of the sample and then fits to a single exponential (Cumulants analysis ISO 13321) (Fig. S3†) yielding the mean hydrodynamic diameter and PDI. To examine the EE of **PF8NT2/6**, the as-prepared nanoparticles were centrifuged at 4 °C (12 000 rpm, 30 min) and the supernatant was collected to measure the amount of free **PF8NT2/6** (non-encapsulated **PF8NT2/6**) using UV-Vis-NIR spectrometer (Agilent Technologies, Cary 5000, USA) at 610 nm. All measurements were performed in triplicate. The EE (%) was then calculated as the following equation:

$$\text{EE } (\%) = \left(\frac{W_{\text{initial}} - W_{\text{free}}}{W_{\text{free}}}\right) \times 100 \quad (1)$$

where W_{initial} and W_{free} are weight of initial **PF8NT2/6** and **PF8NT2/6** detected in supernatant after centrifugation respectively.[20]

Morphology of the **PCL-PF8NT2/6** nanoparticles was investigated using Transmission Electron Microscopy (TEM, JEM-2100, JEOL, Japan) operated at an accelerating voltage of 200 kV. Size distribution of the nanoparticles was analysed from TEM imaging ($n = 50$) using image processing program (ImageJ). Elemental analysis was done using an Energy Dispersive X-ray Spectrometer (EDS) detector equipped with TEM. For specimen preparation, a few drops of the diluted sample were deposited on a carbon coated copper grid without staining and air dried overnight. Composition of the nanoparticles was investigated through thermogravimetric analysis (TGATGA/DSC 3+, Mettler Toledo, Switzerland). The samples were heated from 25 to 700 °C using a heating rate of 10 °C min^{-1} under nitrogen atmosphere. NIR fluorescence spectra of the prepared nanoparticles were recorded using NIR spectroscopy (QuantaMaster™ 500, Photon Technologies International, USA) at excitation wavelength (λ_{ex}) of 610 nm and emission spectra recorded in range of 700–1200 nm. All measurements were performed in 1 cm quartz cell with the excitation and emission slit of 10 nm at room temperature. Flow cytometer (FACScanto II, BD) was also applied for determination of homogeneity of fluorescence emission of the **PCL-PF8NT2/6** nanoparticles.

2.3.3. *In vitro* cytotoxicity of PCL-PF8NT2/6 nanoparticles. Colony-forming technique was carried out according to ISO 10993 Part 5 to ascertain the viability of mouse fibroblast cells, NCTC clone 929 [L-929, derivative of Strain L] (ATCC® CCL-1™) treated with the **PCL-PF8NT2/6** nanoparticles.[21] First, L-929 cells were cultured in RPMI completed medium (Bibco). Cells were stained with trypan blue exclusion technique and the number of living cells was determined with hemacytometer using an optical microscope (CKX41, Olympus, Japan).

The **PCL-PF8NT2/6** nanoparticles (0.1 g) were separately diluted using the completed medium (1 mL), *i.e.* RPMI-1640 supplemented with HEPES (25 mM), D-glucose (1.8 mg mL^{-1}), glutamine (2 mM), gentamicin (40 mg mL^{-1}) and 10% heat-inactivated fetal calf serum (FCS) to attain a given concentration. L-929 cells were seeded at the density of 100 cells per well in 24-well plates and incubated for 24 h (37 °C, 5% CO_2). After incubation for 6 days, the number of colonies on each well was counted under the optical microscope and % inhibition of cell growth was evaluated. Culture medium was used instead of the encapsulated nanoparticles in the case of negative control. Statistical significance was evaluated using one-way analysis of variance (ANOVA) (Minitab). Results with p-values < 0.05 were considered to be statistically significant.

3. Results and discussion

3.1. Preparation of PCL-PF8NT2/6 nanoparticles

With the aim to apply the synthesized **PCL-PF8NT2/6** nanoparticles in biomedical applications, it is expected that the monodisperse nanoparticles possess high stability and cell compatibility. Herein the encapsulation of hydrophobic **PF8NT2/6** NIR dye into a polymer matrix was carried out by way of an emulsion–diffusion technique as this offers monodispersed particles with high encapsulation efficiency of active compounds (generally >70%) from preformed polymer. This process exhibits a high batch-to-batch reproducible manner and ease of scale-up.[22,23] Generally, this method uses ethyl acetate (water solubility 8.3 g/100 mL at 20 °C, dielectric constant 6.0) as an organic solvent to dissolve polymers and the active molecules.[24,25] However, in our study, very hydrophobic **PF8NT2/6** dye cannot be completely dissolved in ethyl acetate. Chloroform (water solubility 0.809 g/100 mL at 20 °C, dielectric constant 4.8) was used instead to dissolve the NIR dye and **PCL** yielded a blue transparent mixture.[26] Firstly, the partially water-soluble chloroform was saturated with DI water ensuring an initial thermodynamic equilibrium of both liquids which can avoid mass-transfer during the process.[27] The reaction began after the addition of surfactant dissolved in chloroform-saturated water into water-saturated chloroform containing a mixture of **PCL** and NIR dye under ultrasonic treatment. After adding water in the dilution step, chloroform continuously

flowed away from initial homogeneous droplets of **PCL-PF8NT2/6**-chloroform stabilized with non-ionic surfactant to the aqueous-rich phase. This gave rise to polymer aggregation and consequently formed solid **PCL-PF8NT2/6** nanoparticles.[27,28] Moinard-Chécot suggested that the advantage of eliminating organic solvent using the diffusion process (water addition) is the fact that it is milder than the direct evaporation as the nanodispersion does not directly resist mechanical stress inside the aqueous suspension during the evaporation.[25]

It is noteworthy that a surfactant is a critical preparative variable to obtain the stable nanoparticles and can affect the formation mechanism, as well as surface characteristics of the prepared nanoparticles.[29] In this study, various biocompatible non-ionic surfactants, including Tween® 80 (small molecule surfactant), PVA and Kolliphor® P188 (polymeric surfactant) with different hydrophilic–lipophilic balance (HLB) values, were employed in the preparation process. Surfactants with high HLB values correspond to the high hydrophilic/lipophobic characteristics of the molecule.[30] Hydrodynamic diameter, PDI and zeta potential of the encapsulated nanoparticles prepared using those surfactants at the same concentration of **PCL** (10 mg) and **PF8NT2/6** NIR dye (1 mg) are summarized in Table 1.

As shown in Table 1, when using polymeric surfactants, PVA or Kolliphor® P188, the prepared **PCL-PF8NT2/6-2** and **PCL-PF8NT2/6-3** exhibited a drastically higher hydrodynamic diameter of 282.7 and 285.7 nm compared to that using Tween® 80 (**PCL-PF8NT2/6-1**). This might be attributed to the small molecular size of Tween® 80 which can lower surface tension at the oil–water interface compared to that of polymeric surfactant (PVA and Kolliphor® P188) at the same concentration. This led to reduction of particle sizes during the emulsification step which encourages solvent diffusion to the aqueous phase during dilution and evaporation steps resulted in small size nanoparticles.[31] However, upon short-term storage, precipitation of **PCL-PF8NT2/6-1** in aqueous medium can be observed.[32] This indicates a low efficiency of Tween® 80 at a given concentration for stabilization of the prepared nanoparticles. Based on emulsion–diffusion technique, it has been believed that a stable nanoparticle would generate if the sufficient surfactant remains on the interface area and adequately protects the globule from coalescence or aggregation during dilution step.[29] In the case of Kolliphor® P188, poly(ethylene glycol)-*block*-poly(propylene glycol)-*block*-poly(ethylene glycol) (PEG-*b*-PPG-*b*-PEG), this block copolymer acts as steric stabilizer in a manner where the hydrophobic PPG chain aligns on the surface of the nanoparticles and the other two hydrophilic PEG chains extend into the aqueous phase. This structure promotes steric repulsion to prevent droplet aggregation during **PCL-PF8NT2/6-3** formation.[33,34] In addition, the high HLB value of Kolliphor® P188 indicates the strong tendency to migrate at oil/water interface and then stabilized the prepared nanoparticles, as well as lowering the exchange rate of entrapped **PF8NT2/6** dye to the surrounding aqueous solution.[32] Although PVA and Kolliphor® P188 are non-ionic polymeric surfactants, higher HLB values of Kolliphor® P188 can stabilize smaller, more uniform and homogeneous emulsion droplets compared to PVA. This led to the low PDI value of **PCL-PF8NT2/6-3**. In addition, larger PDI values of the **PCL-PF8NT2/6-2** may attribute to high extent of hydrolysis of PVA (99+% hydrolyzed), inducing strong intermolecular and intramolecular hydrogen bonding occurrence in PVA chain. This results in a low efficiency of PVA to prevent the globule coalescence by steric stabilization during solvent diffusion process.[25,33,35] These results suggest that the structure of the surfactant is a factor that significantly influences hydrodynamic diameter and PDI of the prepared **PCL-PF8NT2/6** nanoparticles.

According to Table 1, it can be seen that the zeta potential of all **PCL-PF8NT2/6** nanoparticles exhibited slightly negative values. This relates to dissociation of hydrophilic –COOH end group of **PCL**. During the dilution step, the migration of chloroform in the **PCL** matrix to the chloroform-saturated aqueous phase possibly encourages the re-arrangement of **PCL** by moving the hydrophobic part of **PCL** chain close to the oil and water interface.[29,36] In addition, using TGA technique, two steps thermal degradation of **PCL-PF8NT2/6-2** and **PCL-PF8NT2/6-3** (320–440 °C and 460–600 °C) compared to neat **PCL** and **PF8NT2/6** were observed (Fig. S4†).[37] The data implied the presence of **PF8NT2/6** encapsulated in **PCL** matrix.

Based on intrinsic characteristics of **PF8NT2/6**, the fluorescence intensity of the prepared **PCL-PF8NT2/6** nanoparticles was investigated in comparison to free **PF8NT2/6** dye at λ_{ex} of 610 nm, as presented in Fig. 1.

As can be seen in Fig. 1, the prepared **PCL-PF8NT2/6-2** and **-3** exhibited two obvious maximum emission wavelengths (λ_{max}) (at 841 and 918 nm for **PCL-PF8NT2/6-2** and 840 and 921 nm for **PCL-PF8NT2/6-3**), which resembled the λ_{max} of free **PF8NT2/6** NIR dye at 843 and 922 nm. Significant lower fluorescence intensity of **PCL-PF8NT2/6-1** might be originated from the low amount of the dye encapsulated in the **PCL** matrix due to the low efficiency of Tween® 80 to stabilize the nanoparticles as mentioned above. It is worth noting that λ_{max} of **PCL-PF8NT2/6-2** and **-3** nanoparticles at approximately 840 nm is in the NIR optical window (between 700–900 nm in wavelength), enabling deeper tissue penetration with a higher signal-to-background

Table 1 Hydrodynamic diameter, PDI and zeta potential of the PCL-PF8NT2/6 nanoparticles prepared using different surfactants

Sample	Surfactant	HLB	Hydrodynamic diameter[a] (nm)	PDI[a]	Zeta potential[a] (mV)
PCL-PF8NT2/6-1	Tween® 80	15	21.2 ± 1.3	0.65 ± 0.02	−5.52 ± 0.44
PCL-PF8NT2/6-2	PVA	18	282.7 ± 4.3	0.51 ± 0.04	−1.55 ± 0.06
PCL-PF8NT2/6-3	Kolliphor® P188	29	285.7 ± 4.9	0.25 ± 0.01	−6.65 ± 0.44

[a] Each value represents the mean ± SD ($n = 3$).

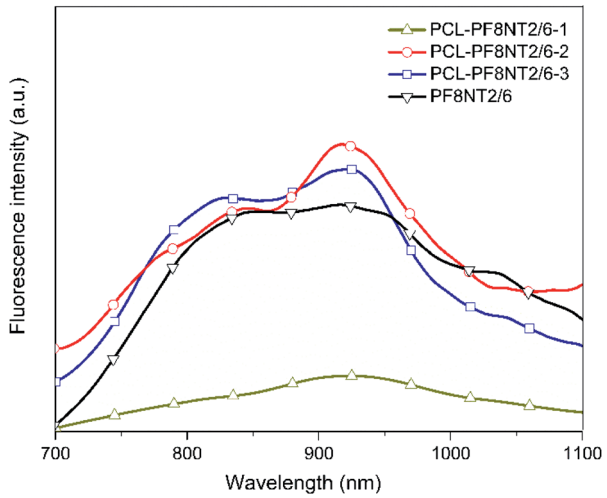

Fig. 1 Fluorescence spectra of free **PF8NT2/6** NIR dye (0.05 mg mL^{-1} in chloroform) and **PCL-PF8NT2/6** nanoparticles (0.05 mg mL^{-1} in DI water) prepared using different surfactants (λ_{ex} = 610 nm).

ratio.[38] Ding *et al.* noted that the emission wavelength of far-red/near-infrared fluorescent conjugated polymer (CP) nanoparticles is 600–800 nm (λ_{max} = 698 nm) and can be utilized as a fluorescent probe for bio-imaging applications.[39] The red-shift of emission spectra of CP nanoparticles is attributed to the increased conjugation system.[40] The quantum yield of **PCL-PF8NT2/6-1**, **2** and **3** nanoparticles measured using indocyanine green (ICG) dye dissolved in DMSO as a reference was found to be 0.9, 1.6 and 3.3%, respectively. Although the fluorescent intensity of **PCL-PF8NT2/6-2** and **-3** nanoparticles was quite similar, PDI and stability of **PCL-PF8NT2/6-2** measured from the DLS was lower than that of **PCL-PF8NT2/6-3**. Therefore, Kolliphor® P188 block copolymer was found to be a suitable surfactant for preparing the **PCL-PF8NT2/6** nanoparticles in this system.

3.2. Influence of PF8NT2/6 concentration on optical and colloidal characteristics of PCL-PF8NT2/6 nanoparticles

Dye concentration is an important factor yielding high fluorescent intensity, colloidal stability and EE of the nanoparticles. In this study, initial concentration of the **PF8NT2/6** was varied from 0.25 to 2.0 mg while keeping other parameters including concentrations of **PCL** and surfactant, reaction temperature and time constant.

Optical characteristics of the **PCL-PF8NT2/6-3** nanoparticles with various amount of dye were investigated using UV-vis absorption and NIR photoluminescence. Fig. 2a shows the absorption spectra of the aqueous suspension of the encapsulated nanoparticles as a function of dye concentration. All **PCL-PF8NT2/6-3** nanoparticles exhibit the two maximum absorption peaks at wavelengths of 400 and 645 nm. The absorbance increases with increasing dye concentration which relates to color intensity of the prepared nanoparticles, as displayed in Fig. 2b. The absorption peak at 400 nm is attributed to π–π* transition of the conjugated backbone of the **PF8NT2/6** dye,

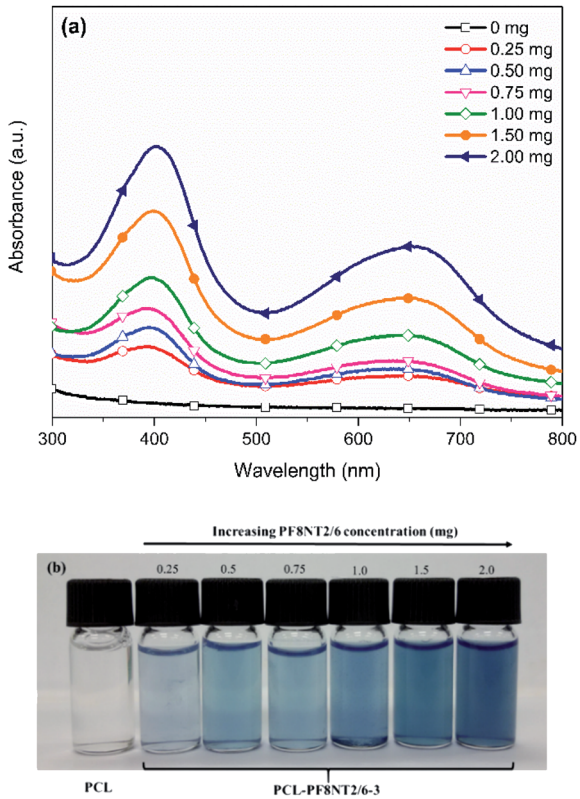

Fig. 2 (a) UV-vis absorption spectra and (b) photographs of the **PCL-PF8NT2/6-3** nanoparticles at different dye concentrations.

while the broad absorption peak at 550–700 nm is resulted from charge transfer between fluorene and naphthalene units of dye molecule.[41] It can be noticed that the fluorescence signal from the **PCL-PF8NT2/6-3** nanoparticles is detectable upon excitation at 610 nm, indicating that most excited electrons return to the ground state *via* radiative decay.[42] Fig. 3 shows the near IR photoluminescence spectra of the prepared nanoparticles suspended in DI water. As can be seen in Fig. 2a and 3, the **PCL-**

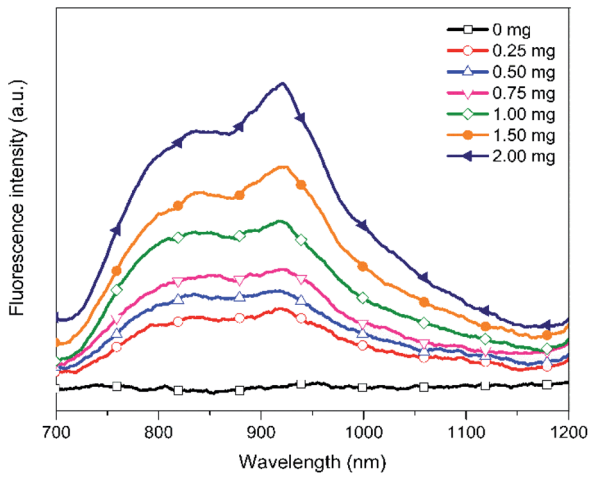

Fig. 3 Fluorescence intensity of the **PCL-PF8NT2/6-3** nanoparticles in aqueous media at different dye concentrations.

PF8NT2/6-3 nanoparticles present the absorption peak at 645 nm and the emission maximum peak at 921 nm with an obvious large Stokes shift of 276 nm. This value is remarkably larger than the previously reported NIR conjugated dye nanoparticles.[39,43] Slight red-shift of absorption and the emission peaks can be observed when the concentration of **PF8NT2/6** was increased. These results are in line with the previous research reported by Wu *et al.*, in which the shift of spectra is probably due to the aggregation of dye which is attributed to the dye molecules getting close to each other inside the nanoparticle.[44] Additionally, the encapsulated nanoparticles exhibit the increasing fluorescence intensity of two emission peaks (837 and 919 nm) when the dye concentration increased, as shown in Fig. 3. These results reveal that there is an increasing number of dye molecules in the **PCL** matrix.

Hydrodynamic diameter, PDI and zeta potential of the synthesized **PCL-PF8NT2/6-3** at various dye concentrations are displayed in Table 2.

As shown in Table 2, the hydrodynamic diameter of **PCL-PF8NT2/6-3** nanoparticles tends to increase with increasing NIR dye concentration. Bare **PCL** nanoparticles exhibit the smallest diameter and highest PDI, indicating its inhomogeneous size distribution.

However, after loading **PF8NT2/6** dye, the PDI of the nanoparticles decreases, especially when using **PF8NT2/6** concentration in the range of 0.5 to 1.5 mg. Increasing dye concentration higher than 1.5 mg caused the formation of large aggregates of the excess dye in aqueous phase which can be seen *via* the naked eye. Considering the absolute zeta potential of the **PCL-PF8NT2/6-3** nanoparticles, an increase in the absolute value is observed compared to that of the bare **PCL** nanoparticles. However, the value does not significantly differ as the dye concentration increased. These nanoparticles are stabilized owing to the steric repulsion of the hydrophilic part of Kolliphor® P188 extending into aqueous phase.[45] The near neutral surface charges of these synthesized **PCL-PF8NT2/6-3** nanoparticles would be advantageous for *in vivo* use as the large positive or negative charges can lead to rapid blood clearance.[46]

Based on eqn (1), EE of the **PCL-PF8NT2/6-3** nanoparticles prepared using various concentrations of the dye are summarized in Table 2. Our results indicate that EE increased up to 82.8% with increasing the dye concentration from 0.25 to 2.0 mg. This result agrees well with the photographs of the **PCL-PF8NT2/6-3** shown in Fig. 2b. Since the structure of the **PF8NT2/6** molecule is quite hydrophobic, its interaction with **PCL** chain and consequential encapsulation is preferable. Although the use of 2.0 mg NIR dye showed the highest EE of 82.8%, its PDI value indicated low homogeneity of nanoparticles. Monodisperse particles are an important requirement to understand the physical property (size and shape) of nanoparticles and to minimize the variability in biological application.[47] Therefore, an optimal concentration of **PF8NT2/6** NIR dye giving high fluorescence intensity, EE, as well as low PDI value, is 1.5 mg. Fluorescence intensity histogram obtained from flow cytometer in Fig. 4b clearly demonstrates homogeneity of fluorescence emission of **PCL-PF8NT2/6-3** nanoparticles (1.5 mg of **PF8NT2/6**) compared with that of bare **PCL** in Fig. 4a at the same particle concentration. The histogram shifts more to the right-hand side compared to that of **PCL** nanoparticles (Fig. 4a), suggesting a strong fluorescence signal of these **PCL-PF8NT2/6-3** nanoparticles, which could provide a sufficient fluorescence signal for cell labelling.

Morphology and elemental composition of the **PCL-PF8NT2/6-3** nanoparticles (1.5 mg of NIR dye) was investigated using TEM equipped with EDS. Results are displayed in Fig. 5.

As can be seen in Fig. 5a, the prepared **PCL-PF8NT2/6-3** nanoparticles (1.5 mg of **PF8NT2/6**) are spherical in shape with mean diameter ranged from 110 to 350 nm. Size distribution analysed from TEM image demonstrates a uniform particle size distribution of the nanoparticles (Fig. S6†) which corresponds to its low PDI value, as shown in Table 2. Theoretically, the dried size observed by TEM is smaller than that measured by DLS

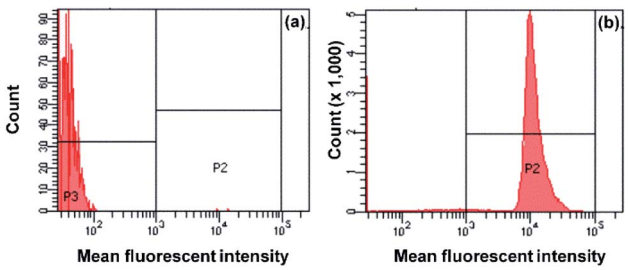

Fig. 4 Fluorescence intensity histogram determined by flow cytometer of (a) bare PCL nanoparticles and (b) PCL-PF8NT2/6-3 nanoparticles at 1.5 mg of NIR dye.

Table 2 Characteristics of the synthesized PCL-PF8NT2/6-3 nanoparticles using different initial concentration of PF8NT2/6

Amount of dye (mg)	Hydrodynamic diameter[a] (nm)	PDI	Zeta potential[a] (mV)	EE (%)
0.0	179.1 ± 6.0	0.49 ± 0.03	−4.77 ± 0.39	—
0.25	265.7 ± 12.6	0.41 ± 0.02	−8.83 ± 0.30	12.5 ± 6.4
0.5	261.6 ± 2.1	0.25 ± 0.01	−7.75 ± 0.51	64.5 ± 4.0
0.75	259.6 ± 1.7	0.25 ± 0.03	−8.62 ± 0.42	67.7 ± 6.5
1.0	285.7 ± 4.9	0.25 ± 0.01	−6.65 ± 0.44	70.4 ± 2.4
1.5	285.0 ± 6.7	0.26 ± 0.01	−8.38 ± 0.67	75.9 ± 6.3
2.0	297.7 ± 5.6	0.41 ± 0.02	−7.59 ± 0.28	82.8 ± 3.5

[a] Each value represents the mean ± SD ($n = 3$).

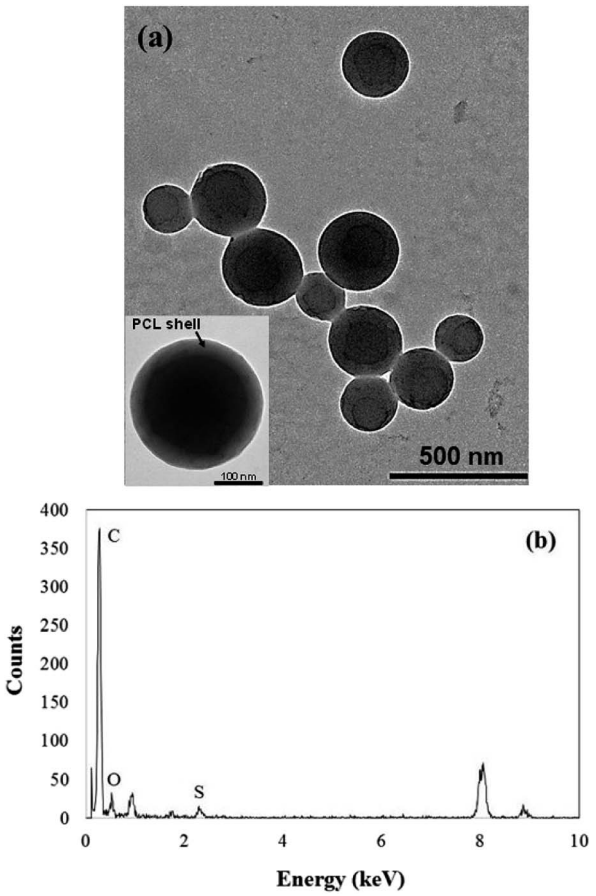

Fig. 5 (a) TEM and high-magnification TEM micrographs (inset) and (b) EDS spectrum of PCL-PF8NT2/6-3 nanoparticles (1.5 mg of NIR dye).

involving the shrinkage of hydrophilic part (PEO chain) of Kolliphor® P188 in dried state. In addition, there is a distinct difference in the contrast of dye (dark core) and **PCL** (light shell) having thickness approximately 36–39 nm, indicating that most **PF8NT2/6** were preferentially located inside the nanoparticle as previously reported.[24,48] Results obtained from EDS in Fig. 5b confirm the presence of sulphur at 2.307 keV which is an element composed only in **PF8NT2/6** compared to that of **PCL** nanoparticles (Fig. S7†).

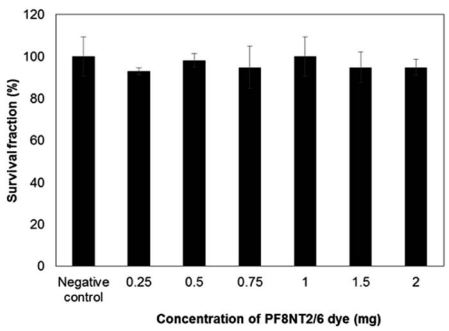

Fig. 6 Percentage of survival fraction of the PCL-PF8NT2/6-3 nanoparticles at various dye concentration on L-929 fibroblast cells after 6 days exposures. Untreated cells or negative control was similarly incubated. Error bar represents mean ± SD of 3 separated sample (at concentration of 0.025 mg mL^{-1}).

3.3. *In vitro* cytotoxicity of the PCL-PF8NT2/6-3 nanoparticles

With the aim to apply this nanoparticle in biomedical applications, the cytotoxic effect of the **PCL-PF8NT2/6-3** nanoparticles was evaluated. Proliferation capacity of a single cell in the presence of the **PCL-PF8NT2/6-3** nanoparticles prepared at various dye concentrations was studied based on colony-forming efficiency assay using L-929 fibroblast cell line. In RPMI culture media composed of protein and salt components, the **PCL-PF8NT2/6-3** nanoparticles demonstrate good stability as their hydrodynamic diameter is close to that in original synthesis media (Fig. S8†). Changes in cell viability after incubation with the samples result in a reduction of the number of colonies formed compared to a negative control. The percentages of survival fraction as a function of NIR dye concentration are depicted in Fig. 6.

As can be seen in Fig. 6, after 6 days' exposure to the **PCL-PF8NT2/6-3**, the percentage of survival fraction of L-929 cells was higher than 90% irrespective of concentration of **PF8NT2/6** dye. The values do not significantly differ from negative control ($P < 0.05$). Slight negative charges of these nanoparticles may not drastically affect cell viability as it has been reported that positively charged particles likely interact with negatively charged portions of cell membrane inducing toxicity response *via* endocytosis.[49] An almost neutral charge of the synthesized **PCL-PF8NT2/6-3** might hinder them from getting internalization through the cell membrane. In addition, Kolliphor® P188 is defined as a FDA approved surfactant and suitable for human use. The zeta potential of the **PCL-PF8NT2/6-3** at various NIR dye concentrations is quite similar, so that survival fraction was not remarkably different. It has been previously described that dynamic layer of protein corona occurred from interaction between cell culture media components and nanoparticles diminished the toxic response to the cells.[50] A similar contribution was possibly observed in this study. Additionally, the adsorbed proteins might increase the colloidal stability of the nanoparticles by taking part in their stabilization *via* steric stabilization. These results highlighted that the synthesized nanoparticles are not toxic to L-929 cells at this investigated concentration.

4. Conclusions

We have successfully synthesized the NIR fluorescent dye (**PF8NT2/6**) encapsulated into **PCL** matrix *via* emulsion–diffusion technique. Using Kolliphor® P188 as a surfactant, the prepared **PCL-PF8NT2/6-3** nanoparticles exhibited a spherical morphology and uniform size distribution. Increasing dye concentration gave rise in absorbance and fluorescence intensity of the nanoparticles. Remarkably, a large Stokes shift of 276 nm in aqueous medium was obtained. These results reveal the **PCL-PF8NT2/6-3** nanoparticles with great potential to diminish background interference for bio-imaging

applications. Finally, the results from the colony-forming technique demonstrated low toxicity of the nanoparticles to the cells irrespective of **PF8NT2/6** concentration.

Conflicts of interest

The authors declare no conflict of interest.

Acknowledgements

This research was supported by National Nanotechnology Center, National Science and Technology Development Agency (NSTDA) (P1450519). K. J. is grateful to Mahidol University for research support. The Authors thank the Center for Research and Innovation, Faculty of Medical Technology, Mahidol University for facility support.

References

1 M. Kolitz-Domb, I. Grinberg, E. Corem-Salkmon and S. Margel, Engineering of near infrared fluorescent proteinoid-poly(L-lactic acid) particles for in vivo colon cancer detection, *J. Nanobiotechnol.*, 2014, **12**, 30–42.

2 T. Behnke, L. E. Mathejczyk, R. Brehm, C. Würth, F. R. Gomes, C. Dullin, J. Napp, F. Alves and U. Resch-Genger, Target-specific nanoparticles containing a broad band emissive NIR dye for the sensitive detection and characterization of tumor development, *Biomaterials*, 2013, **34**, 160–170.

3 Z. Yang, S. Zheng, W. J. Harrison, J. Harder, X. Wen, J. G. Gelovani, A. Qiao and C. Li, Long-circulating near-infrared fluorescence core-cross-linked polymeric micelles: synthesis, characterization, and dual nuclear/optical imaging, *Biomacromolecules*, 2007, **8**, 3422–3428.

4 S. M. Yoon, S. J. Myung, I. W. Kim, E. J. Do, B. D. Ye, J. H. Ryu, K. Park, K. Kim, I. C. Kwon, M. J. Kim, D. H. Moon, D. H. Yang, K. J. Kim, J. S. Byeon, S. K. Yang and J. H. Kim, Application of Near-infrared fluorescence imaging using a polymeric nanoparticle-based probe for the diagnosis and therapeutic monitoring of colon cancer, *Dig. Dis. Sci.*, 2011, **56**, 3005–3013.

5 A. Topete, M. Alatorre-Meda, P. Iglesias, E. M. Villar-Alvarez, S. Barbosa, J. A. Costoya, P. Taboada and V. Mosquera, Fluorescent drug-loaded, polymeric-based, branched gold nanoshells for localized multimodal therapy and imaging of tumoral cells, *ACS Nano*, 2014, **8**, 2725–2738.

6 A. Yuan, J. Wu, X. Tang, L. Zhao, F. Xu and Y. Hu, Application of near-infrared dyes for tumor imaging, photothermal, and photodynamic therapies, *J. Pharm. Sci.*, 2013, **102**, 6–28.

7 S. Luo, E. Zhang, Y. Su, T. Cheng and C. Shi, A review of NIR dyes in cancer targeting and imaging, *Biomaterials*, 2011, **32**, 7127–7138.

8 X. Yi, F. Wang, W. Qin, X. Yang and J. Yuan, Near-infrared fluorescent probes in cancer imaging and therapy: an emerging field, *Int. J. Nanomed.*, 2014, **9**, 1347–1365.

9 M. Laine, N. A. Barbosa, A. Kochel, B. Osiecka, G. Szewczyk, T. Sarna, P. Ziółkowski, R. Wieczorek and A. Filarowski, Synthesis, structural, spectroscopic, computational and cytotoxic studies of BODIPY dyes, *Sens. Actuators, B*, 2017, **238**, 548–555.

10 L. Hu, Z. Yan and H. Xu, Advances in synthesis and application of near-infrared absorbing squaraine dyes, *RSC Adv.*, 2013, **3**, 7667–7676.

11 J. O. Escobedo, O. Rusin, S. Lim and R. M. Strongin, NIR dyes for bioimaging applications, *Curr. Opin. Chem. Biol.*, 2010, **14**, 64–70.

12 J. Zhang, Z. Zhang, B. Yu, C. Wang, W. Wu and X. Jiang, Synthesis and biological properties of porphyrin-containing polymeric micelles with different sizes, *ACS Appl. Mater. Interfaces*, 2016, **8**, 5794–5803.

13 K. Hoffmann, T. Behnke, D. Drescher, J. Kneipp and U. Resch-Genger, Near-infrared-emitting nanoparticles for lifetime-based multiplexed analysis and imaging of living cells, *ACS Nano*, 2013, **7**, 6674–6684.

14 T. Behnke, C. Würth, K. Hoffmann, M. Hübner, U. Panne and U. Resch-Genger, Encapsulation of hydrophobic dyes in polystyrene micro- and nanoparticles via swelling procedures, *J. Fluoresc.*, 2011, **21**, 937–944.

15 J. Napp, T. Behnke, L. Fischer, C. Würth, M. Wottawa, D. M. Katschinski, F. Alves, U. Resch-Genger and M. Schäferling, Targeted luminescent near-infrared polymer-nanoprobes for in vivo imaging of tumor hypoxia, *Anal. Chem.*, 2011, **83**, 9039–9046.

16 G. Meng, S. Velayudham, A. Smith, R. Luck and H. Liu, Color tuning of polyfluorene emission with BODIPY monomers, *Macromolecules*, 2009, **42**, 1995–2001.

17 D. Neher, Polyfluorene homopolymers: conjugated liquid-crystalline polymers for bright blue emission and polarized electroluminescence, *Macromol. Rapid Commun.*, 2001, **22**, 1365–1385.

18 U. Asawapirom, R. Güntner, M. Forster, T. Farrell and U. Scherf, Dialkylfluorene-oligothiophene and dialkylfluorene-dithienylvinylene alternating copolymers, *Synthesis*, 2002, **9**, 1136–1142.

19 P. Piyakulawat, A. Keawprajak, A. Chindaduang, M. Hanusch and U. Asawapirom, Synthesis and preliminary characterization of novel naphthalene bisimide based copolymers, *Synth. Met.*, 2009, **159**, 467–472.

20 J. Hu, J. Guo, Z. Xie, D. Shan, E. Gerhard, G. Qian and J. Yang, Fluorescence imaging enabled poly(lactide-*co*-glycolide), *Acta Biomater.*, 2016, **29**, 307–319.

21 International Organization for Standardization, *Biological evaluation of medical devices - Part 5: Tests for In Vitro Cytotoxicity*, International Organization for Standardization, Geneva, Switzerland, 2009, ISO 10993-5:2009(en).

22 B. V. N. Nagavarma, K. S. Y. Hemant, A. Ayaz, L. S. Vasuha and H. G. Shivakumar, Different techniques for preparation of polymeric nanoparticles-a review, *Asian J. Pharm. Clin. Res.*, 2012, **5**, 16–23.

23 C. E. Mora-Huertas, H. Fessi and A. Elaissari, Polymer-based nanocapsules for drug delivery, *Int. J. Pharm.*, 2010, **385**, 113–142.

24 M. Choi, A. Soottitantawat, O. Nuchuchua, S. Min and U. Ruktanonchai, Physical and light oxidative properties of eugenol encapsulated by molecular inclusion and emulsion–diffusion method, *Food Res. Int.*, 2009, **42**, 148–156.

25 D. Moinard-Chécot, Y. Chevalier, S. Briançon, L. Beney and H. Fessi, Mechanism of nanocapsules formation by the emulsion–diffusion process, *J. Colloid Interface Sci.*, 2008, **317**, 458–468.

26 S. Lee, E. Yoo, H. Ghim and S. Lee, Alginate nanohydrogels prepared by emulsification-diffusion method, *Macromol. Res.*, 2009, **17**, 168–173.

27 S. Guinebretière, S. Briancon, H. Fessi, V. S. Teodorescu and M. G. Blanchin, Nanocapsules of biodegradable polymers: preparation and characterization by direct high resolution electron microscopy, *Mater. Sci. Eng., C*, 2002, **21**, 137–142.

28 M. Hassou, F. Couenne, Y. Gorrec and M. Tayakout, Modeling and simulation of polymeric nanocapsule formation by emulsion diffusion method, *AIChE J.*, 2009, **55**, 2094–2105.

29 C. E. Mora-Huertas, F. Couenne, H. Fessi and A. Elaissari, Electrokinetic properties of poly-ε-caprolactone-based nanoparticles prepared by nanoprecipitation and emulsification-diffusion methods: a comparative study, *J. Nanopart. Res.*, 2010, **14**, 876–891.

30 R. W. Egan, M. A. Jones and A. L. Lehninger, Hydrophile-lipophile balance and critical micelle concentration as key factors influencing surfactant disruption of mitochondrial membranes, *J. Biol. Chem.*, 1976, **251**, 4442–4447.

31 T. Tadros, P. Izquierdo, J. Esquena and C. Solans, Formation and stability of nano-emulsions, *Adv. Colloid Interface Sci.*, 2004, **108**, 303–318.

32 N. Garti and D. J. McClements, *Encapsulation Technologies and Delivery Systems for Food Ingredients and nutraceuticals*, Woodhead Publishing Limited, Cambridge, 2012.

33 N. Sharma, P. Madan and S. Lin, Effect of process and formulation variables on the preparation of parenteral paclitaxel-loaded biodegradable polymeric nanoparticles: a co-surfactant study, *Asian J. Pharm. Sci.*, 2016, **11**, 404–416.

34 T. Tadros, Polymeric surfactants in disperse systems, *Adv. Colloid Interface Sci.*, 2009, **147**, 281–299.

35 H. Murakami, Y. Kawashima, T. Niwa, T. Hino, H. Takeuchi and M. Kobayashi, Influence of the degrees of hydrolyzation and polymerization of poly(vinylalcohol) on the preparation and properties of poly(DL-lactide-*co*-glycolide) nanoparticle, *Int. J. Pharm.*, 1997, **149**, 43–49.

36 U. Bazylinska, A. Pucek, M. Sowa, E. Matczak-Jon and K. A. Wilk, Engineering of phosphatidylcholine-based solid lipid nanocarriers for flavonoids delivery, *Colloids Surf.*, 2014, **460**, 483–493.

37 M. R. Tavares, L. R. Menezes, J. C. D. Filho, L. M. Cabral and M. I. B. Taveres, Surface-coated polycaprolactone nanoparticles with pharmaceutical application: Structural and molecular mobility evaluation by TD-NMR, *Polym. Test.*, 2017, **60**, 39–48.

38 J. Mérian, J. Gravier, F. Navarro and I. Texier, Fluorescent nanoprobes dedicated to in vivo imaging: from preclinical validations to clinical translation, *Molecules*, 2012, **17**, 5564–5591.

39 D. Ding, J. Liu, G. Feng, K. Li, Y. Hu and B. Liu, Bright far-red/near-infrared conjugated polymer nanoparticles for in vivo bioimaging, *Small*, 2013, **9**, 3093–3102.

40 H. Liu, P. Wu, S. Kuo, C. Chen, E. Chang, C. Wu and Y. Chan, Quinoxaline-based polymer dots with ultrabright red to near-infrared fluorescence for in vivo biological imaging, *J. Am. Chem. Soc.*, 2015, **137**, 10420–10429.

41 J. Geng, C. Sun, J. Liu, L. Liao, Y. Yuan, N. Thakor, J. Wang and B. Liu, Biocompatible conjugated polymer nanoparticles for efficient photothermal tumor therapy, *Small*, 2015, **11**, 1603–1610.

42 C. L. Amiot, S. Xu, S. Liang, L. Pan and J. X. Zhao, Near-infrared fluorescent materials for sensing of biological targets, *Sensors*, 2008, **8**, 3082–3105.

43 K. Li, D. Ding, D. Huo, K. Pu, N. N. Phuong Thao, Y. Hu, Z. Li and B. Liu, Conjugated polymer based nanoparticles as dual-modal probes for targeted in vivo fluorescence and magnetic resonance imaging, *Adv. Funct. Mater.*, 2012, **22**, 3107–3115.

44 W. Wu, C. Chen, Y. Tian, S. Jang, Y. Hong, Y. Liu, R. Hu, B. Tang, Y. Lee, C. Chen, W. Chen and A. K.-Y. Jen, Enhancement of aggregation-induced emission in dye-encapsulating polymeric micelles for bioimaging, *Adv. Funct. Mater.*, 2010, **20**, 1413–1423.

45 Y. Zhang, L. Tang, L. Sun, J. Bao, C. Song, L. Huang, K. Liu, Y. Tian, G. Tian, Z. Li, H. Sun and L. Mei, A novel paclitaxel-loaded poly(ε-caprolactone)/poloxamer 188 blend nanoparticle overcoming multidrug resistance for cancer treatment, *Acta Biomater.*, 2010, **6**, 2045–2052.

46 N. Ramalingam, G. Natesan, B. Dhandayuthapani, P. Perumal, J. Balasundaram and S. Natesan, Design and characterization of ofloxacin niosomes, *Pak. J. Pharm. Sci.*, 2013, **26**, 1089–1096.

47 J. D. Robertson, L. Rizzello, M. Avila-Olias, J. Gaitzsch, C. Contini, M. S. Magoń, S. A. Renshaw and G. Battaglia, Purification of nanoparticles by size and shape, *Sci. Rep.*, 2016, **6**, 27494–27502.

48 K. Lia and B. Liu, Polymer-encapsulated organic nanoparticles for fluorescence and photoacoustic imaging, *Chem. Soc. Rev.*, 2014, **43**, 6570–6597.

49 S. Nandhakumar, M. D. Dhanaraju, V. D. Sundar and B. Heera, Influence of surface charge on the in vitro protein adsorption and cell cytotoxicity of paclitaxel loaded poly(ε-caprolactone) nanoparticles, *Bull. Fac. Pharm.*, 2017, **55**, 249–258.

50 I. Lynch and K. A. Dawson, Protein-nanoparticle interactions, *Nano Today*, 2008, **3**, 40–47.